Adaptive Transformers for Robust Few-shot Cross-domain Face Anti-spoofing

Hsin-Ping Huang[1,2]   **Deqing Sun**[2]   **Yaojie Liu**[2]   **Wen-Sheng Chu**[2]
Taihong Xiao[1,2]   **Jinwei Yuan**[2]   **Hartwig Adam**[2]   **Ming-Hsuan Yang**[1,2]
[1]University of California, Merced   [2]Google Research

Abstract

While recent face anti-spoofing methods perform well under the intra-domain setups, an effective approach needs to account for much larger appearance variations of images acquired in complex scenes with different sensors for robust performance. In this paper, we present adaptive vision transformers (ViT) for robust cross-domain face anti-spoofing. Specifically, we adopt ViT as a backbone to exploit its strength to account for long-range dependencies among pixels. We further introduce the ensemble adapters module and feature-wise transformation layers in the ViT to adapt to different domains for robust performance with a few samples. Experiments on several benchmark datasets show that the proposed models achieve both robust and competitive performance against the state-of-the-art methods for cross-domain face anti-spoofing using a few samples.

1 Introduction

Face biometrics is widely applied to identity authentication applications due to its security, convenience, and no-contact nature, compared to conventional methods such as passcodes and fingerprints [26]. Other than face recognition, there is an additional step needed to keep the authentication systems secure from spoof presentation attacks, which is called face anti-spoofing. For example, printed photos, digital images, and 3D masks can deceive mobile platforms to authenticate the attacker as the genuine user, which would cause severe security breach. As a result, face anti-spoofing has been an important topic with studies for almost two decades.

In early systems, face authentication is mainly applied to controlled scenarios with fixed sensors such as building access and border control. With controlled environments and limited variations (*e.g.*, lighting and poses), all faces can be regarded as from one single domain. Numerous simple yet effective methods [4, 10, 32] can be applied to determine whether spoof attacks occur or not. Recently, mobile applications such as unlock and payment have increased the risk of spoofing attacks. Face images may be acquired from wider angles, complex scenes, and different devices, which can be regarded as a set of mixed data domains. In addition, an anti-spoof module may be deployed to new devices (*i.e.*, unseen domains). Accordingly, face anti-spoofing is required to not only handle large variations, but also well generalize or quickly adapt to unseen scenes and sensors.

Existing methods use intra-database testing and cross-database testing to evaluate the intra-domain and cross-domain face anti-spoofing performance. The former one trains and evaluates models on data splits from the same database, while the latter one does from different databases. Recent methods have already shown saturated performance on intra-database evaluations [1, 4, 3] in well-controlled scenarios. In recent years, numerous methods have been proposed to tackle cross-domain face anti-spoofing [48, 40, 22]. Although significant progress has been made, existing methods do not perform well on cross-dataset tests, *e.g.*, on CASIA, intra-testing *vs.* cross-testing can be 0% *vs.* 10% on half total error rate. Thus, it is of great interest to develop robust anti-spoofing methods for cross-domain scenarios.

Preprint. Under review.

There are a few challenges for cross-domain face anti-spoofing applications:

- **Domain gap.** The domain gap is highly correlated to the key factor of recognizing spoof: visual appearance. Spoofing cues, such as moire pattern and color distortion, can dramatically change or disappear with different camera devices, illuminations, and image resolutions. For example, images from Oulu-NPU [5] are in 1080P resolution, while images from Idiap Replay [9] are only in 480P resolution. The sensor noise and low image quality of Idiap Replay can lead to a biased prediction as spoof from a model trained on Oulu-NPU.
- **Limited data.** Compared to datasets for other vision tasks, *e.g.*, CelebA[42] and FFHQ[23], commonly used datasets for face anti-spoofing (such as CASIA[80], Idiap Replay[9], MSU-MFSD[64], and Oulu-NPU[5]) are considerably smaller in scale. Hence, models trained with limited data can easily over-fit the training data, and thereby generalize poorly to other domains. It is similar to training a model for downstream object recognition tasks with limited data but no ImageNet pre-trained modules.

In this work, we address these challenges and propose a robust cross-domain model that performs as well as for intra-domain tasks. The proposed model learns to exploit important visual information related to face spoofing from the training data and adapt well to new domains with a few samples. Specifically, we introduce the vision transformer [13] as the backbone module for cross-domain face anti-spoofing. To facilitate cross-domain adaption with a few samples, we propose adaptive transformers by integrating ensemble adapter modules and feature-wise transformation layers. Extensive experimental results show our proposed models outperform the state-of-the-art method on the widely-used benchmark datasets. We also provide insightful analysis on why the proposed adaptive transformer outperforms the evaluated methods. The main contributions of this work are:

- We propose adaptive transformers with ensemble adapters and feature-wise transforms for robust cross-domain face anti-spoofing with a few samples.
- We achieve state-of-the-art cross-domain face anti-spoofing results on widely-used benchmark datasets. Our approach closes the gap between intra-database evaluation and performance in real-world applications.
- We conduct in-depth analysis of adaptive transformers and show model explainability with insights for face anti-spoofing.

2 Related Work

Face anti-spoofing. Early works exploit spontaneous human behaviors (*e.g.*, eye blinking, head motion) [25, 46] or predefined movements (*e.g.*, head turning, expression changes) [8] to address face anti-spoofing. Due to the clear weaknesses in video replaying attacks and the inconvenience from user interaction, recent approaches evolve into modeling material properties (*i.e.*, texture). Several methods utilize hand-crafted features to describe spoof related patterns, *e.g.*, LBP [4, 10], HoG [27, 68] and SIFT [48] features, and train a live/spoof classifier using support vector machines or linear discriminant analysis. More recently, deep neural networks have been applied to anti-spoofing [53, 40, 41, 75, 22] and achieved state-of-the-art performance than conventional methods [67, 14, 32, 47].

As limited spoof data is available for learning classifiers or deep neural networks, auxiliary supervisory signals have been introduced to infuse the models with prior knowledge, such as facial depth map [39], rPPG signal [36], reflection [70], and face albedo [43]. To improve model interpretability, feature disentanglement is proposed along with advances in generative adversarial networks [41, 75]. Furthermore, customized deep network architectures are shown to be more effective for face anti-spoofing, *e.g.*, tree-like structure [40], network architecture search [73, 71].

Most recently, a model based on a vision transformer is proposed to detect spoofing attack [16]. Although this transformer-based method is able to detect certain spoofs, it does not perform well on challenging print and replay attacks (*e.g.*, 5.84/15.20 [16] *vs.* 2.1/10.0 [40] EER on SiW-M dataset). These results suggest large headroom to improve models in detecting low-level texture cues. In this work, we propose an adaptive transformer model to robustly handle challenging print and replay spoof attacks across different datasets using a few-shot setting (*i.e.*, as few as 5 samples).

Domain generalization. Domain generalization for face anti-spoofing aims to learn a model from multiple source datasets, and the model should generalize to the unseen target dataset. Several
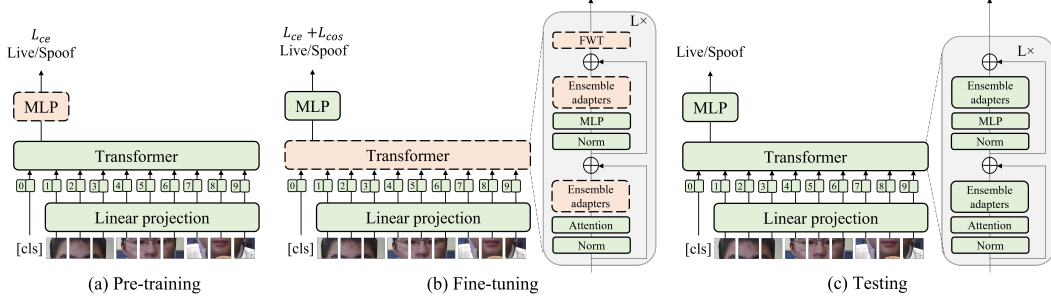
Figure 1: **Overview of our robust cross-domain face anti-spoofing framework.** The module or layer colored in wheat or green means that the weights are trainable or fixed. The transformer receives image patches and an extra learnable classification embedding [cls] as inputs, and a multi-layer perceptron (MLP) is used for live/spoof face classification. At the pre-training stage (a), the backbone is fixed and only the MLP head is trained using L_{ce}. At the fine-tuning stage (b), we insert two ensemble adapter modules and a feature-wise transformation (FWT) layer to each transformer block, and train all ensemble adapters and FWT layers using $L_{ce} + L_{cos}$ when other layers are fixed. During testing (c), the FWT layers are removed from the model.

approaches [53, 22, 52, 24] based on adversarial training and triplet loss have been developed to learn a shared feature space for multiple source domains that can generalize to the target domain. On the other hand, meta-learning formulations [54, 7, 62] are exploited to simulate the domain shift at training time to learn a representative feature space. Furthermore, disentangled representation for spoof and ID features [61] and sample re-weighting [38] improve generalization for face anti-spoofing. In contrast, we tackle a real-world anti-spoofing problem when only a few images are available from target datasets. In this work, we propose an effective cross-domain few-shot framework based on an adaptive transformer that achieves state-of-the-art performance.

Few-shot learning. Few-shot learning methods [20, 63, 2, 55, 56, 60, 15, 51] aim to adapt models to novel classes from a few samples from each class (assuming the classes used for training are disjoint with the novel classes seen at test time). Cross-domain few-shot learning [78, 19, 58] further addresses the problem when the novel classes are sampled from a different domain with different data distribution. In contrast, few-shot supervised domain adaptation aims to adapt models to new domains with the assistance of a few examples [44, 57, 65, 45].

Anti-spoofing methods based on few-shot and zero-shot learning [50, 40] are proposed to detect multiple spoof attacks. The SASA method [66] studies a similar cross-domain problem by using a few target samples to better generalize, and the features are learned within the adversarial learning framework. As shown in [66], cross-domain model performance is unstable under different protocols. In contrast, we propose to learn features from balanced data from the source domains and a few samples from the target domain. We also propose an adaptive transformer based on an adapter and a feature-wise transformation to improve the model stability.

3 Method

In this work, we assume that there exist N source datasets $\mathbf{S} = \{\mathcal{S}_1, \mathcal{S}_2, \mathcal{S}_3, \ldots, \mathcal{S}_N\}$ from different domains and one target dataset $\mathcal{T}$, where each source dataset $\mathcal{S}_i$ consists of real and fake images $\mathcal{S}_i = \{X_r^{\mathcal{S}_i}, X_f^{\mathcal{S}_i}\}$. The goal of few-shot cross-domain anti-spoofing is to learn a classification model that generalizes to the target domain $\mathcal{T}$ by accessing source datasets $\mathbf{S}$ as well as a few samples (*e.g.*, 5 samples) from the target set $\mathcal{T}' = \{X_r^{\mathcal{T}'}, X_f^{\mathcal{T}'}\} \subseteq \mathcal{T}$.

To achieve this goal, we propose a robust framework based on the vision transformer (ViT) [13] and the adaptive modules for few-shot cross-domain face anti-spoofing. The proposed approach consists of three components: vision transformer, ensemble adapters and feature-wise transformation. Fig. 1 shows the overall framework, and Fig. 2 presents the adaptive modules. We describe each component in the following sections.

3

$$L_{cos}(\widehat{\mathbf{h}}^i, \widehat{\mathbf{h}}^j)$$

$\widehat{\mathbf{h}}^i$ $\oplus$ $\widehat{\mathbf{h}}^j$

Linear (m, n) Linear (m, n)

GELU   GELU

Linear (n, m) Linear (n, m)
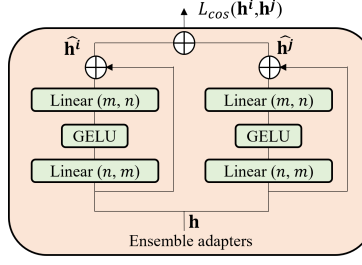
h

Ensemble adapters

Figure 2: **Ensemble adapters.** The ensemble adapters contain multiple adapters which take the same hidden representation as inputs, and the outputs of multiple adapters are aggregated. A cosine similarity loss is applied to pairs of outputs of adapters to enforce each adapter to learn diverse representations that complement with each other. Each adapter is a bottleneck layer with skipped connections. When the training starts, the adapter layers are close to identity layers, and they can be adapted for face anti-spoofing task or retained as the identity function.

3.1 Vision Transformer

We adopt the vision transformers (ViT) [13] as our backbone module to tackle the face anti-spoofing problem. Following the standard pipeline of ViT training, we split and reshape the input image into a sequence of flattened 2D patches. To retain the positional information, we prepend learnable positional embedding to the patch embedding. We use ViT to obtain the image representations and a multi-layer perceptron (MLP) head to get the classification prediction, *i.e.*, whether the input image is a live or a spoof face.

At each training iteration, we form a balanced batch by sampling the same amount of live and spoof images from N source domain and a small subset of target domain $\{X_r^{\mathcal{S}_i}, X_f^{\mathcal{S}_i}, X_r^{\mathcal{T}'}, X_f^{\mathcal{T}'}\}$, where the sample size is B. The model prediction is $\{\hat{y}_r^{\mathcal{S}_i}, \hat{y}_f^{\mathcal{S}_i}, \hat{y}_r^{\mathcal{T}'}, \hat{y}_f^{\mathcal{T}'}\}$. We use the cross entropy loss L_{ce} to train our model, which is defined by

$$L_{ce} = \frac{1}{B(N+1)} \sum_{j=1}^{B} \left(\sum_{i=1}^{N} (\log(\hat{y}_{r_j}^{\mathcal{S}_i}) + \log(1 - \hat{y}_{f_j}^{\mathcal{S}_i})) + \log(\hat{y}_{r_j}^{\mathcal{T}'}) + \log(1 - \hat{y}_{f_j}^{\mathcal{T}'}) \right). \quad (1)$$

Unlike other object classification tasks where holistic information plays an essential role, we need to detect local spoof-related cues appearing possibly all over the image for the face anti-spoofing problem. Empirically, it has been shown that patch-based face anti-spoofing methods [3, 69] improve the performance as the network extracts more discriminative local features by using patches as inputs. However, these methods use convolutional neural networks to extract patch features and predict spoof scores for each patch independently. Furthermore, they use global pooling to fuse the scores for final prediction, which fails to apply global reasoning by considering the correlation among patches. In contrast, ViT captures the long-range dependency among different patches via the global self-attention mechanism. As a result, the local spoof-related cues can be detected independently and accumulated globally for better spoof predictions. Therefore, ViT is suitable for face anti-spoofing.

3.2 Ensemble Adapters

One straightforward transfer learning strategy is to train a classifier on top of features extracted by a backbone network pre-trained on ImageNet [11] using anti-spoofing data. However, this strategy yields poor performance on the face anti-spoofing task for two reasons. First, the backbone pre-trained using a generic dataset cannot adapt well to the specific anti-spoofing facial data. Second, features extracted from the pre-trained backbone network are high-level, thus not suitable for the face anti-spoofing task where the subtle low-level information is crucial.

Instead, one can fine-tune a classifier and the backbone on anti-spoofing data. Although good performance could be achieved on the source domain, the performance on the target domain becomes unstable even when the training loss approaches convergence as shown in Fig. 3 and Section 4.3. We attribute the instability to two factors. 1) When fine-tuning large models with few samples, the

catastrophic forgetting problem usually causes training instability. 2) The domain gap between the target samples and the source domain is large such that the target samples are close to the decision boundary and have high uncertainty. An intuitive remedy is to freeze a majority of the backbone and partially fine-tune the network. However, the approach with fine-tuning only top layers of backbone networks does not address this issue. In the following, we propose to use ensemble adapter layers to achieve stable cross-domain performance.

Adaptive module. In natural language processing, the adapterBERT [21] has been shown to successfully transfer the pre-trained BERT model to various downstream tasks without re-training the whole network. In this work, we introduce the adapter layer to alleviate the instability issue. The adapter has a bottleneck architecture containing few parameters relative to the feedforward layers. As shown in Fig. 2, it first linearly projects the n-dimensional features into a lower dimension m, applies a non-linear activation function GELU, and then projects back to n dimensions. As the adapter also contains a skip-connection, it is nearly an identity function if the parameters of the projection head are initialized to near-zero. As shown in Fig. 1(b), two adaptive modules are inserted into each transformer block. During the fine-tuning stage, we fix the original transformer backbone and update the weights of adaptive modules. As adapters contain only a few parameters ($\approx 3\%$ parameters of the original model), they can be learned without optimization difficulties. Thanks to the skip-connections, the adapters generate representations with less deviation from the pre-trained models and alleviate the catastrophic forgetting problem, thereby improving training stability. Adapters also help adjust the feature distribution of the pre-trained transformer blocks to the face anti-spoofing data, maintaining the discriminative strength and good generalization ability of pre-trained transformer representations.

Ensemble adapters and cosine similarity loss. In this work, we introduce the ensemble adapters module to achieve higher accuracy and minimize training instability issues. Instead of having two naive adapters in each transformer block, we insert two ensemble adapter modules in each block. The ensemble adapters contain K adapters in parallel. Specifically, in each ensemble adapter module, the representation $\mathbf{h}$ is the input to K adapters and the outputs of adapters $\hat{\mathbf{h}}^k$ are aggregated and forwarded to the next layer. However, by simply ensembling the adapter outputs, multiple adapters learn repetitive information which does not improve the discriminability of the features and leads to limited performance improvements. In order to learn diverse features from multiple adapters, we use a cosine similarity loss which constrains multiple outputs of adapters to be complementary. Specifically, we minimize the cosine distance between each pair of outputs of the adapters $\hat{\mathbf{h}}^i$ and $\hat{\mathbf{h}}^j$. The cosine loss enforces the outputs of adapters to be dissimilar to each other and help learn diverse features. Assume the input image has N tokens and the feature dimension is D, we compute the cosine distance along the feature dimension and average over the number of tokens N. The cosine loss L_{cos} is defined by

$$\hat{\mathbf{h}} = \sum_{k=1}^{K} \hat{\mathbf{h}}^k = \sum_{k=1}^{K} Adapter_k(\mathbf{h}), \tag{2}$$

$$L_{cos} = \sum_{1 \leq i,j \leq K, i \neq j} \frac{1}{N} \sum_{n=1}^{N} \left(\frac{\hat{\mathbf{h}}_n^i \cdot \hat{\mathbf{h}}_n^j}{\left\| \hat{\mathbf{h}}_n^i \right\| \left\| \hat{\mathbf{h}}_n^j \right\|} \right)^2. \tag{3}$$

As the ensemble is conducted at the bottleneck network, our ensemble module is lightweight. Adding each additional adapter requires $\approx 3\%$ additional FLOPs and parameters, which are relatively low overheads. In practice, our model takes 15% additional inference time compared to naive ViT.

3.3 Feature-wise Transformation

Our goal is to learn a model that generalizes well to the target domain using source datasets and a small subset of the target dataset. Due to the distribution mismatch of the source and target domains, the model is prone to over-fitting since we only have access to limited target domain data during training. Thus, we include a feature-wise transformation (FWT) layer [58] into the transformer blocks. As shown in Fig. 2, we first sample the scaling and bias terms of affine transformations from

Gaussian distributions,

$$\alpha^d \sim N(0, \text{softplus}(W_\alpha^d)), \quad d = 1, \ldots, D, \tag{4}$$

$$\beta^d \sim N(0, \text{softplus}(W_\beta^d)), \quad d = 1, \ldots, D, \tag{5}$$

where W_α^d and W_β^d denote learnable sampling hyper-parameters, and D denotes the channel dimension of the activation map of each transformer block. We then compute the modulated features by applying the sampled affine transformations to intermediate features of layer $\mathbf{x}_l$ as follows:

$$\hat{\mathbf{x}}_l = \mathbf{x}_l + \boldsymbol{\alpha}_l \cdot \mathbf{x}_l + \boldsymbol{\beta}_l, \quad l = 1, \ldots, L. \tag{6}$$

In practice, the same affine transformation is applied across all patch embeddings.

As shown in Fig. 1(b), we insert one FWT layer in each transformer block. The FWT layer is used only at training time as augmentation, and not used at test time. The FWT layer serves as feature-level data augmentation to increase the diversity of training samples, thus dramatically reducing overfitting and improving stability and performance. The FWT layer is complementary to image-level augmentation and we apply both to help model training at the same time.

3.4 Adaptive Transformer

The proposed adaptive transformer consists of three stages: pre-training, fine-tuning and testing, as shown in Fig. 1. At the pre-training stage, we fix the ViT backbone initialized with pre-trained weights from ImageNet [11] and train the MLP head using the binary cross entropy loss L_{ce}. At the fine-tuning stage, we insert two ensemble adaptor modules and an FWT layer to each transformer block, and train all ensemble adaptors and FWT layers with all the other weights fixed until convergence using cross entropy loss and cosine loss $L_{ce} + L_{cos}$. During the testing stage, we remove the FWT layers and keep ensemble adaptors for cross-domain classification.

4 Experiments

4.1 Experimental Setups

Datasets and protocols. Two evaluation protocols are used in this work. In **Protocol 1**, we provide evaluations on four widely-used benchmark datasets: CASIA [80], Idiap Replay attack [9], MSU-MFSD [64], and Oulu-NPU [5]. Following the prior works, we regard each dataset as one domain and apply the leave-one-out testing protocol to evaluate the cross-domain generalization. In **Protocol 2**, we conduct similar cross-domain evaluations on the larger-scale datasets: CASIA-SURF [77, 76], CASIA-CeFA [33, 34], and WMCA [17]. Compared to datasets in **Protocol 1**, datasets in **Protocol 2** have much more subjects and richer environment variations, and thus the results can better reflect model performance. In both protocols, we include CelebA-Spoof [79] as the supplementary training data to increase the diversity of training samples to learn better spoof representations.

Implementation details. The input images are cropped and resized to $224 \times 224 \times 3$ and split into a patch size of 16×16. We use an Adam optimizer with an initial learning rate of 1e-4 and weight decay of 1e-6. The batch size is 8 for each training domain. We use ViT-Base as our backbone whose output embedding dimension is 768, and the MLP head contains two fully-connected layers whose dimensions are 512 and 2. The adapter layers have dimension $n = 768$ and $m = 64$. We set the number of ensemble adapters $K = 2$ in the experiments. More experimental results of the ensemble adapters are in the supplementary materials. We first train the MLP head for 100 iterations in the pre-training stage and then the ensemble adapters and FWT layers for 4000 iterations in the fine-tuning stage. Our method is implemented using Pytorch. The source code and trained models will be made available to the public.

Evaluation metrics. We evaluate the model performance using three metrics: Half Total Error Rate (HTER), Area Under Curve (AUC), and True Positive Rate (TPR) at a fixed False Positive Rate (FPR). While HTER and AUC assess the theoretical performance, TPR at a certain FPR is adept at reflecting how well the model performs in practice. We use TPR@FPR=1% as the metric which is a high usability setting.

Table 1: Evaluation of cross-domain face anti-spoofing among CASIA (**C**), Replay (**I**), MSU-MFSD (**M**), and Oulu-NPU (**O**) databases. Methods are compared at their best performance based on the evaluation process in [22]. SSDG† denotes the cross-domain performance reported in [22] without using CelebA-Spoof as the supplementary source dataset.

	Method	OCI → M			OMI → C			OCM → I			ICM → O		
		HTER	AUC	TPR@FPR=1%	HTER	AUC	TPR@FPR=1%	HTER	AUC	TPR@FPR=1%	HTER	AUC	TPR@FPR=1%
0-shot	NAS-FAS [73]	16.85	90.42	–	15.21	92.64	–	11.63	96.98	–	13.16	94.18	–
	DRDG [38]	12.43	95.81	–	19.05	88.79	–	15.56	91.79	–	15.63	91.75	–
	D^2AM [7]	12.70	95.66	–	20.98	85.58	–	15.43	91.22	–	15.27	90.87	–
	Self-DA [62]	15.40	91.80	–	24.50	84.40	–	15.60	90.10	–	23.10	84.30	–
	ANRL [37]	10.83	96.75	–	17.85	89.26	–	16.03	91.04	–	15.67	91.90	–
	FGHV [35]	9.17	96.92	–	12.47	93.47	–	16.29	90.11	–	13.58	93.55	–
0-shot	SSDG† [22]	7.38	97.17	–	10.44	95.94	–	11.71	96.59	–	15.61	91.54	–
	SSDG	6.58	97.21	48.33	12.91	93.92	56.43	**7.01**	**98.28**	**63.85**	12.47	94.87	51.55
	ViT	**1.58**	**99.68**	**96.67**	**5.70**	**98.91**	**88.57**	9.25	97.15	51.54	**7.47**	**98.42**	**69.30**
5-shot	SSDG	8.42	97.39	63.33	12.91	93.59	60.71	4.48	99.14	80.77	7.81	97.46	67.61
	ViT	3.42	98.60	95.00	1.98	99.75	94.00	2.31	99.75	87.69	7.34	97.77	66.90
	ViTA	4.75	98.84	76.67	5.00	99.13	82.14	5.37	98.57	76.15	7.16	97.97	73.24
	ViTAF	3.42	99.30	88.33	1.40	99.85	95.71	3.74	99.34	85.38	7.17	98.26	71.97
	ViTAF*	**2.92**	**99.62**	**91.66**	**1.40**	**99.92**	**98.57**	**1.64**	**99.64**	**91.53**	**5.39**	**98.67**	**76.05**

Table 2: Evaluation on cross-domain protocols among CASIA-SURF (**S**), CASIA-CeFA (**C**), and WMCA (**W**) databases. Methods are compared at their best performance based on the evaluation process in [22].

	Method	CS → W			SW → C			CW → S		
		HTER	AUC	TPR@FPR=1%	HTER	AUC	TPR@FPR=1%	HTER	AUC	TPR@FPR=1%
0-shot	SSDG	12.64	94.35	55.72	12.25	94.78	**51.67**	27.08	80.05	12.06
	ViT	**7.98**	**97.97**	**73.61**	**11.13**	**95.46**	47.59	**13.35**	**94.13**	**49.97**
5-shot	SSDG	5.08	99.02	77.49	6.72	98.11	74.28	18.88	88.25	23.42
	ViT	4.30	99.16	83.55	7.69	97.66	68.33	12.26	94.40	42.59
	ViTA	3.77	99.42	85.78	6.02	98.47	78.29	15.67	91.86	51.21
	ViTAF	4.51	99.44	88.23	7.21	97.69	70.87	11.74	94.13	50.87
	ViTAF*	**2.91**	**99.71**	**92.65**	**6.00**	**98.55**	**78.56**	**11.60**	**95.03**	**60.12**

Evaluation against state-of-the-art methods. We evaluate our model against the state-of-the-art cross-domain face anti-spoofing SSDG [22] method under several settings:

- 0-shot SSDG†: we do not add CelebA-Spoof, which is under the same setting as the SSDG paper [22].
- 0-shot SSDG: CelebA-Spoof is included as one of the source domains.
- 5-shot SSDG: CelebA-Spoof is included as one of the source domains, and the 5-shot samples are included at training time.

We include reported results of recent 0-shot methods in Table 1 for completeness. These methods do not outperform our SSDG baseline model. We are not able to evaluate these methods in the few-shot settings as the codes are not released.

Proposed methods. We include these variants of our methods for evaluation:

- ViT: a ViT is used as the backbone, and the whole backbone along with the MLP layer are updated during training.
- ViTF: a ViT with FWT layers is used as the backbone, and the whole network along with the MLP layer are updated during training.
- ViTA: a ViT with naive single adapters is used as the backbone. Only the adapter layers are updated during training.
- ViTAF: a ViT with naive single adapters and FWT layers is used as the backbone. Only the adapter and FWT layers are updated during training.
- ViTAF*: a ViT with ensemble adapters and FWT layers is used as the backbone. The ensemble adapters and FWT layers are updated during training.

4.2 Cross-domain Performance

Table 1 and Table 2 show the cross-domain performance for **Protocol 1** and **Protocol 2** respectively. **Effectiveness of CelebA-Spoof.** As shown in Table 1, the 0-shot SSDG model outperforms 0-shot

SSDG[†] on three out of four targets, which results in an average improvement of 0.76 AUC. The improvement can be attributed to two reasons. First, the CelebA-Spoof dataset can increase the diversity of source domain training data. Therefore, the distance between some source samples and the target samples is reduced, which benefits the cross-domain classification. Second, using more diverse training data could smooth the decision boundary and result in better model generalization ability.

0-shot performance. ViT outperforms SSDG on AUC scores for six out of total seven target domains: M (+2.5), C (+5.0), O (+3.6), W (+3.6), C (+0.7), S (+14.1), except for I (-1.1). The result shows that ViT is a strong backbone that generalizes better to the unseen target datasets. A ViT backbone fine-tuned on the source datasets with only a standard cross entropy loss can achieve competitive performance upon baseline approaches that employ special domain generalization techniques such as triplet loss and adversarial training. We also find that adding additional triplet loss or adversarial learning does not bring performance gain to the ViT backbone.

From 0-shot to 5-shot. 5-shot SSDG improves upon 0-shot SSDG for six out of seven target domains with an average of 2.78 AUC. Similarly, 5-shot ViT improves upon 0-shot ViT for five out of seven target domains with an average of 0.77 AUC. These results demonstrate that using only 5-shot samples can effectively adapt the model to the target domain. Due to camera devices, illuminations, and image resolutions, a large domain gap exists between the source and target domains. In this case, a few target samples can effectively reveal some crucial characteristics and differences between live and spoof faces of the target domain, thereby facilitating the model adaptation to the target domain. It is worth noticing that 5-shot test samples are a relatively small subset in terms of dataset size, taking 4.7/1.6/1.2/0.3% of the target domain data in **Protocol 1** and approximately 0.1% of the target domain data in **Protocol 2**.

5-shot performance. ViTA outperforms 5-shot SSDG for six out of seven target domains: M (+1.45), C (+5.54), O (+0.51), W (+0.40), C (+0.35), S (+3.60), except for I (-0.57). Combining adapters and FWTs, the ViTAF model outperforms 5-shot SSDG for six out of seven target domains: M (+1.90), C (+6.26), O (+0.80), I (+0.20), W (+0.42), S (+5.88), except for C (-0.42).

Comparison of ViTA and ViTAF. Comparing ViTA with ViTAF, FWT layers achieves consistent improvement for **Protocol 1**: M (+0.46), C (+0.72), I (+0.77), O (+0.29). For **Protocol 2**, ViTAF achieves improvements only for the S domain (+2.28). This is likely due to the smaller size of datasets in **Protocol 1**, which highlights the importance of FWT layers to generate a more diverse distribution and increase the dataset size.

Comparison of ViTAF and ViTAF[*]. With the ensemble adapters, our full model ViTAF[*] achieves consistent improvement for all the targets over ViTAF: M (+0.32), C(+0.07), I(+0.30), O(+0.41), W(+0.27), C(+0.86), S(+0.90). The results show that the ensemble adapters and the cosine similarity loss facilitate learning diverse features from multiple adapters which are complementary with each other. Overall, our model achieves state-of-the-art results for all target domains, demonstrating the effectiveness of our method to adapt the model to the target domain with few samples. We further discuss the variants of our method in the following section.

4.3 Ablation Study

We conduct ablation studies to analyze the contributions of each module using the 5-shot setting and **Protocol 1**. As discussed in Section 3.2, the performance of 5-shot ViT model may fluctuate among different checkpoints even the training loss converges. The best performance among all the checkpoints is reported in Table 1 and 2, following [22]. In Fig. 3, we show the average AUC and standard deviation of the last eight checkpoints when the training process converges. Although the *best* performance of ViT is good in Table 1, the performance fluctuates and has lower *average* performance in Fig. 3. Comparing ViT with ViTF, ViTA and ViTAF, both FWT layers and adapter layers achieve better *average* performance with smaller standard deviation for all targets. Our full model ViTAF[*] achieves the best performance with the lowest standard deviation, which validates the robust performance achieved by the ensemble adapters.
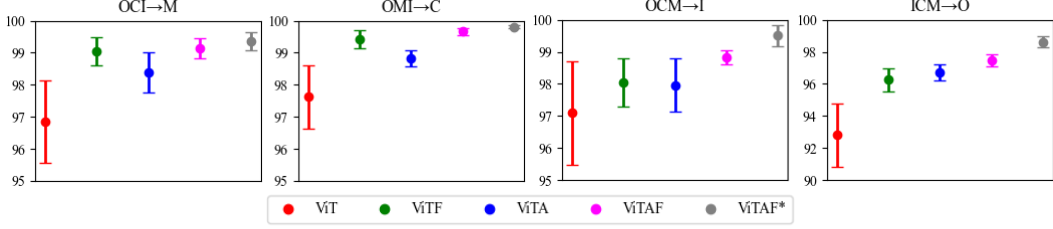
Figure 3: **Ablation study.** We analyze different components of our model including ensemble adapter layers and feature-wise transformation (FWT) layers. We report the average AUC and standard deviation of the last eight checkpoints when the training is converged. The naive adapter and the FWT layer (ViTA, ViTF, ViTAF) both improve the performance. Our ensemble adapters (ViTAF*) further boost the average test performance and the stability.
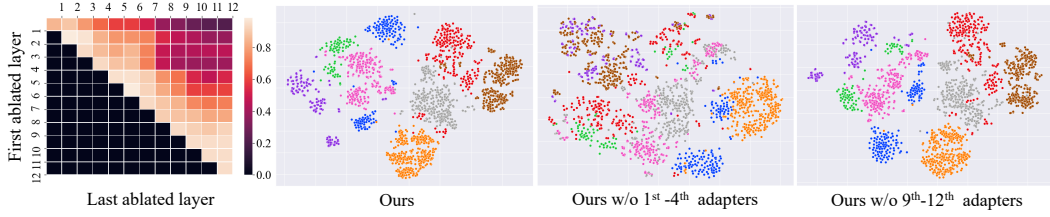

Figure 4: **Visualization of adapter.** We visualize the TPR@FPR=1% score of ablated continuous adapter layers in the left-most sub-figure. The vertical and horizontal dimensions denote the first and last ablated layers. For example, the value at the second row in the fifth column represents the model performance by removing the adapters from the second to fifth layers. We find that ablating a single adapter layer (the diagonal elements) does not lead to much performance drop, while ablating more adapter layers (the upper triangular) causes a larger performance drop. In addition, removing the adapters in the first four layers (the top left) causes a relatively severe performance drop than in the last four layers (the bottom right). We also plot the feature distribution in the three figures to the right. A unique color represents the live or spoof sample from each domain. We can observe that the data samples are less separable by removing the adapters in the first four layers than the last four layers.

4.4 Visualization

Adapter. Fig. 4 shows the TPR@FPR=1% score of ablated continuous adapter layers. The vertical and horizontal dimensions denote the first and last ablated layers. For example, the value at the second row in the fifth column represents the model performance by removing the adapter from the second to fifth layers. All lower triangular values are not required to be considered and thus set to 0. The diagonal numbers are generally good, indicating that ablating a single adapter layer does not affect model performance significantly. On the other hand, removing more adapter layers causes performance drops, which can be verified by the numbers in the upper triangular region. Moreover, the numbers at the top left are relatively smaller than those at the bottom right, which indicates that removing the adapters in the first few layers causes a more significant performance drop while removing the adapters in the last few layers does not.

We further plot the feature distribution using t-SNE [59]. We can observe that samples of all categories are well separated in our method. Moreover, we find that removing adapters in the first four layers leads to less separable distribution than the last four layers. These results show that the low-level features of the transformer are more critical than high-level features for the anti-spoofing task.

Feature-wise transformation. Fig. 5 shows the magnitude of the learned sampling parameters of FWT layers. We can observe that the values of both the scaling and the bias terms are closer to the initial values in deeper layers (9th-12th) and adjusted more in shallower layers (1st-4th), suggesting that the adaptation occurs mainly in the low-level features. This result also coincides with the findings in Fig. 4.
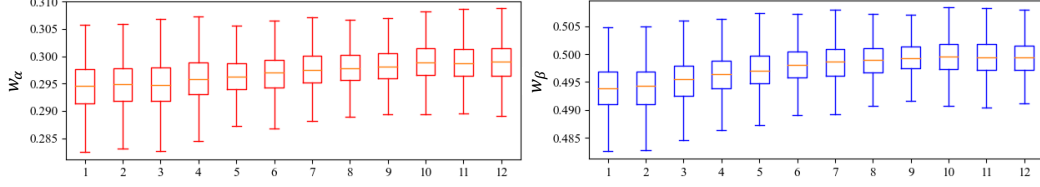
Figure 5: **Visualization of the feature-wise transformation layers.** We present the quartile plot of learned sampling parameters W_α^d and W_β^d of all FWT layers. The box edges in each column mark the 25th and 75th percentiles of all $D = 768$ values. Note that W_α^d and W_β^d are initialized as 0.3 and 0.5, respectively. The values in shallow layers (1st-4th) deviate more from the initial values than those in deep layers (9th-12th), which suggests that the low-level features are adapted more and influence more to the target task.

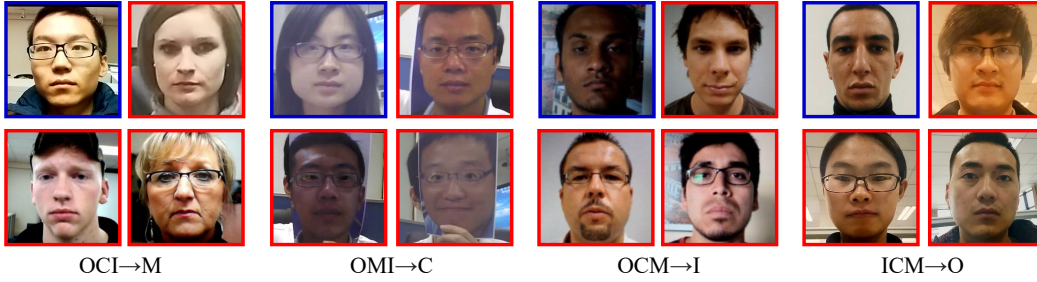OCI→M   OMI→C   OCM→I   ICM→O

Figure 6: **Failure cases of our method.** The live faces misclassified as spoof faces are shown in blue boxes and the spoof faces misclassified as live faces are shown in red boxes. The live faces classified as spoof faces (blue) are mostly in special light conditions or low-quality sensors, suggesting that our method still suffers from domain-specific environments. The spoof faces classified as live faces (red) show that our model has difficulties detecting spoof faces with better visual quality than live faces, detecting the unseen spoof types, and detecting paper attacks with local texture differences.

Failure cases and limitations. Fig. 6 shows the common types of incorrect predictions by our methods. For the live faces classified as spoof faces (blue boxes), the results show that these faces are mostly in special light conditions or captured by low-quality sensors, *e.g.*, strong yellow light (**OCI** → **M**), sensors with weird color temperatures (**OMI** → **C**), dark light (**OCM** → **I**). It suggests that our method still suffers from the domain-specific light condition. Due to the extreme light condition, a live face in one domain may look like a spoof face in another domain. For spoof faces classified as live faces (red boxes), the replay attack displaying a fixed photo is the most challenging type for **OCM** → **I**. These images have even better visual quality than other live images in the same dataset, which causes confusion. Paper attacks are more challenging for **ICM** → **O**, which has the highest resolution among all datasets. While paper attacks show texture differences, there is no clear region of spoof cues, and thus the high-resolution spoof images in **O** may look closer to live images in other datasets. Paper attacks with real human eyes are challenging for **OMI** → **C**. It is difficult to detect this specific attack that only appears in **C** and does not show up in other datasets, including CelebA-Spoof.

Attention maps. As shown in Fig. 7, we visualize the attention maps of different transformers on spoof images using Transformer Explainability [6]. We observe that different regions are highlighted by transformers to make predictions for different spoof face domains. For example, transformers make predictions mainly based on the bright reflection regions for the replay attack in **OCI** → **M**. For paper attacks, transformers focus on hands and paper boundaries in **OMI** → **C**, and the background paper texture in **OCM** → **I**. As for the replay attack in **ICM** → **O**, transformers pay more attention to the background shadows. Moreover, our model can better capture the spoof cues compared to the naive ViT, as the attention region are more conspicuous.

10

| 0-shot ViT | 5-shot ViT | Ours | Input | | 0-shot ViT | 5-shot ViT | Ours | Input |

OCI→M   OMI→C
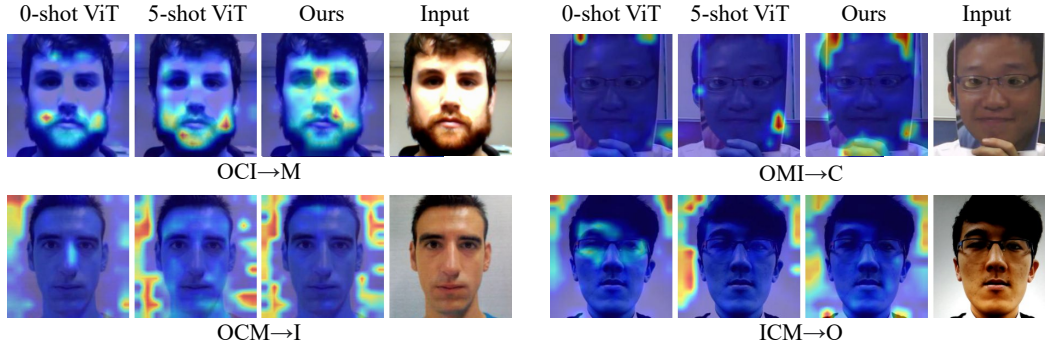
OCM→I   ICM→O

Figure 7: **Transformer attention on spoof images.** We visualize the attention maps of transformers using Transformer Explainability [6]. Transformers focus on face regions with a bright reflection for MSU, hand and paper boundaries for CASIA, background paper textures for Replay, and background shadows for Oulu-NPU. Our model generates more accurate and conspicuous attention maps to capture spoof cues compared with naive ViTs.

5   Conclusion

In this work, we study the task of cross-domain face anti-spoofing with a few samples. We introduce vision transformer with ensemble adapters and feature-wise transforms to adapt to new domains. The proposed ensemble adapters significantly facilitate both stable training process and consistent model performance. Experiments on widely-used benchmark datasets validate that our method achieves state-of-the-art performance for few-shot cross-domain face anti-spoofing.

References

[1] Akshay Agarwal, Richa Singh, and Mayank Vatsa. Face anti-spoofing using haralick features. In *International Conference on Biometrics Theory, Applications and Systems (BTAS)*, 2016. 1

[2] Anthreas Antoniou, Amos Storkey, and Harrison Edwards. Data augmentation generative adversarial networks. In *International Conference on Learning Representations (ICLR)*, 2018. 3

[3] Yousef Atoum, Yaojie Liu, Amin Jourabloo, and Xiaoming Liu. Face anti-spoofing using patch and depth-based cnns. In *International Joint Conference on Biometrics (IJCB)*, 2017. 1, 4

[4] Zinelabidine Boulkenafet, Jukka Komulainen, and Abdenour Hadid. Face anti-spoofing based on color texture analysis. In *International Conference on Image Processing (ICIP)*, 2015. 1, 2

[5] Zinelabinde Boulkenafet, Jukka Komulainen, Lei Li, Xiaoyi Feng, and Abdenour Hadid. Oulu-npu: A mobile face presentation attack database with real-world variations. In *International Conference on Automatic Face & Gesture Recognition (FG)*, 2017. 2, 6

[6] Hila Chefer, Shir Gur, and Lior Wolf. Transformer interpretability beyond attention visualization. In *IEEE Conference on Computer Vision and Pattern Recognition (CVPR)*, 2021. 10, 11, 22

[7] Zhihong Chen, Taiping Yao, Kekai Sheng, Shouhong Ding, Ying Tai, Jilin Li, Feiyue Huang, and Xinyu Jin. Generalizable representation learning for mixture domain face anti-spoofing. In *Association for the Advancement of Artificial Intelligence (AAAI)*, 2021. 3, 7, 15

[8] Girija Chetty. Biometric liveness checking using multimodal fuzzy fusion. In *IEEE International Conference on Fuzzy Systems (FUZZ-IEEE)*, 2010. 2

[9] Ivana Chingovska, André Anjos, and Sébastien Marcel. On the effectiveness of local binary patterns in face anti-spoofing. In *Proceedings of the International Conference of Biometrics Special Interest Group (BIOSIG)*, 2012. 2, 6

[10] Tiago de Freitas Pereira, André Anjos, José Mario De Martino, and Sébastien Marcel. LBP-TOP based countermeasure against face spoofing attacks. In *Asian Conference on Computer Vision (ACCV)*, 2012. 1, 2

[11] Jia Deng, Wei Dong, Richard Socher, Li-Jia Li, Kai Li, and Li Fei-Fei. Imagenet: A large-scale hierarchical image database. In *IEEE Conference on Computer Vision and Pattern Recognition (CVPR)*, 2009. 4, 6, 20

[12] Jesse Dodge, Gabriel Ilharco, Roy Schwartz, Ali Farhadi, Hannaneh Hajishirzi, and Noah A. Smith. Fine-tuning pretrained language models: Weight initializations, data orders, and early stopping. *arXiv preprint arXiv:2002.06305*, 2020. 16

[13] Alexey Dosovitskiy, Lucas Beyer, Alexander Kolesnikov, Dirk Weissenborn, Xiaohua Zhai, Thomas Unterthiner, Mostafa Dehghani, Matthias Minderer, Georg Heigold, Sylvain Gelly, et al. An image is worth 16x16 words: Transformers for image recognition at scale. In *International Conference on Learning Representations (ICLR)*, 2021. 2, 3, 4

[14] Litong Feng, Lai-Man Po, Yuming Li, Xuyuan Xu, Fang Yuan, Terence Chun-Ho Cheung, and Kwok-Wai Cheung. Integration of image quality and motion cues for face anti-spoofing: A neural network approach. *Journal of Visual Communication and Image Representation*, 38:451–460, 2016. 2

[15] Chelsea Finn, Pieter Abbeel, and Sergey Levine. Model-agnostic meta-learning for fast adaptation of deep networks. In *International Conference on Machine Learning (ICML)*, 2017. 3

[16] Anjith George and Sébastien Marcel. On the effectiveness of vision transformers for zero-shot face anti-spoofing. In *International Joint Conference on Biometrics (IJCB)*, 2021. 2

[17] Anjith George, Zohreh Mostaani, David Geissenbuhler, Olegs Nikisins, André Anjos, and Sébastien Marcel. Biometric face presentation attack detection with multi-channel convolutional neural network. *IEEE Transactions on Information Forensics and Security*, 15:42–55, 2020. 6

[18] Golnaz Ghiasi, Tsung-Yi Lin, and Quoc V. Le. Dropblock: A regularization method for convolutional networks. In *Neural Information Processing Systems (NeurIPS)*, 2018. 17

[19] Yunhui Guo, Noel C Codella, Leonid Karlinsky, James V Codella, John R Smith, Kate Saenko, Tajana Rosing, and Rogerio Feris. A broader study of cross-domain few-shot learning. In *European Conference on Computer Vision (ECCV)*, 2020. 3

[20] Bharath Hariharan and Ross Girshick. Low-shot visual recognition by shrinking and hallucinating features. In *IEEE International Conference on Computer Vision (ICCV)*, 2017. 3

[21] Neil Houlsby, Andrei Giurgiu, Stanislaw Jastrzebski, Bruna Morrone, Quentin De Laroussilhe, Andrea Gesmundo, Mona Attariyan, and Sylvain Gelly. Parameter-efficient transfer learning for NLP. In *International Conference on Machine Learning (ICML)*, 2019. 5

[22] Yunpei Jia, Jie Zhang, Shiguang Shan, and Xilin Chen. Single-side domain generalization for face anti-spoofing. In *IEEE Conference on Computer Vision and Pattern Recognition (CVPR)*, 2020. 1, 2, 3, 7, 8, 15

[23] Tero Karras, Samuli Laine, and Timo Aila. A style-based generator architecture for generative adversarial networks. In *IEEE Conference on Computer Vision and Pattern Recognition (CVPR)*, 2019. 2

[24] Taewook Kim and Yonghyun Kim. Suppressing spoof-irrelevant factors for domain-agnostic face anti-spoofing. *IEEE Access*, 2021. 3, 15

[25] Klaus Kollreider, Hartwig Fronthaler, Maycel Isaac Faraj, and Josef Bigun. Real-time face detection and motion analysis with application in "liveness" assessment. *Transactions on Information Forensics and Security (TIFS)*, 2(3):548–558, 2007. 2

[26] Kim Komando. Smartphone security: What's better to use a pin, facial recognition, or your fingerprint? *Fox News*, 2019. 1

[27] Jukka Komulainen, Abdenour Hadid, and Matti Pietikäinen. Context based face anti-spoofing. In *International Conference on Biometrics: Theory, Applications and Systems (BTAS)*, 2013. 2

[28] Aarre Laakso and G. Cottrell. Content and cluster analysis: Assessing representational similarity in neural systems. *Philosophical Psychology*, 13:47 – 76, 2000. 16

[29] Cheolhyoung Lee, Kyunghyun Cho, and Wanmo Kang. Mixout: Effective regularization to finetune large-scale pretrained language models. In *International Conference on Learning Representations (ICLR)*, 2020. 16

[30] Da Li, Yongxin Yang, Yi-Zhe Song, and Timothy M. Hospedales. Deeper, broader and artier domain generalization. In *IEEE International Conference on Computer Vision (ICCV)*, 2017. 17

[31] Hao Li, Zheng Xu, Gavin Taylor, Christoph Studer, and Tom Goldstein. Visualizing the loss landscape of neural nets. In *Neural Information Processing Systems (NeurIPS)*, 2018. 16

[32] Lei Li, Xiaoyi Feng, Zinelabidine Boulkenafet, Zhaoqiang Xia, Mingming Li, and Abdenour Hadid. An original face anti-spoofing approach using partial convolutional neural network. In *International Conference on Image Processing Theory, Tools and Applications (IPTA)*, 2016. 1, 2

[33] Ajian Liu, Zichang Tan, Jun Wan, Sergio Escalera, Guodong Guo, and Stan Z. Li. Casia-surf cefa: A benchmark for multi-modal cross-ethnicity face anti-spoofing. In *Winter Conference on Applications of Computer Vision (WACV)*, 2021. 6

[34] Ajian Liu, Li Xuan, Jun Wan, Yanyan Liang, Sergio Escalera, Hugo Jair Escalante, Meysam Madadi, Yi Jin, Zhuoyuan Wu, Xiaogang Yu, Zichang Tan, Qi Yuan, Ruikun Yang, Benjia Zhou, Guodong Guo, and Stan Li. Cross-ethnicity face anti-spoofing recognition challenge: A review. *IET Biometrics*, 10, 2020. 6

[35] Shice Liu, Shitao Lu, Hongyi Xu, Jing Yang, Shouhong Ding, and Lizhuang Ma. Feature generation and hypothesis verification for reliable face anti-spoofing. In *Association for the Advancement of Artificial Intelligence (AAAI)*, 2022. 7, 15

[36] Siqi Liu, Pong C Yuen, Shengping Zhang, and Guoying Zhao. 3d mask face anti-spoofing with remote photoplethysmography. In *European Conference on Computer Vision (ECCV)*, 2016. 2

[37] ShuBao Liu, Ke-Yue Zhang, Taiping Yao, Mingwei Bi, Shouhong Ding, Jilin Li, Feiyue Huang, and Lizhuang Ma. Adaptive normalized representation learning for generalizable face anti-spoofing. In *ACM International Conference on Multimedia (ACM MM)*, 2021. 7, 15

[38] Shubao Liu, Ke-Yue Zhang, Taiping Yao, Kekai Sheng, Shouhong Ding, Ying Tai, Jilin Li, Yuan Xie, and Lizhuang Ma. Dual reweighting domain generalization for face presentation attack detection. In *International Joint Conference on Artificial Intelligence (IJCAI)*, 2021. 3, 7, 15

[39] Yaojie Liu, Amin Jourabloo, and Xiaoming Liu. Learning deep models for face anti-spoofing: Binary or auxiliary supervision. In *IEEE Conference on Computer Vision and Pattern Recognition (CVPR)*, 2018. 2

[40] Yaojie Liu, Joel Stehouwer, Amin Jourabloo, and Xiaoming Liu. Deep tree learning for zero-shot face anti-spoofing. In *IEEE Conference on Computer Vision and Pattern Recognition (CVPR)*, 2019. 1, 2, 3, 15

[41] Yaojie Liu, Joel Stehouwer, and Xiaoming Liu. On disentangling spoof trace for generic face anti-spoofing. In *European Conference on Computer Vision (ECCV)*, 2020. 2

[42] Ziwei Liu, Ping Luo, Xiaogang Wang, and Xiaoou Tang. Deep learning face attributes in the wild. In *IEEE International Conference on Computer Vision (ICCV)*, 2015. 2

[43] Shlok Kumar Mishra, Kuntal Sengupta, Max Horowitz-Gelb, Wen-Sheng Chu, Sofien Bouaziz, and David Jacobs. Improved detection of face presentation attacks using image decomposition. *arXiv preprint arXiv:2103.12201*, 2021. 2

[44] Saeid Motiian, Quinn Jones, Seyed Iranmanesh, and Gianfranco Doretto. Few-shot adversarial domain adaptation. In *Neural Information Processing Systems (NeurIPS)*, 2017. 3

[45] Saeid Motiian, Marco Piccirilli, Donald A. Adjeroh, and Gianfranco Doretto. Unified deep supervised domain adaptation and generalization. In *IEEE International Conference on Computer Vision (ICCV)*, 2017. 3

[46] Gang Pan, Lin Sun, Zhaohui Wu, and Shihong Lao. Eyeblink-based anti-spoofing in face recognition from a generic webcamera. In *IEEE International Conference on Computer Vision (ICCV)*, 2007. 2

[47] Keyurkumar Patel, Hu Han, and Anil K Jain. Cross-database face antispoofing with robust feature representation. In *Chinese Conference on Biometric Recognition (CCBR)*, 2016. 2

[48] Keyurkumar Patel, Hu Han, and Anil K Jain. Secure face unlock: Spoof detection on smartphones. *Transactions on Information Forensics and Security (TIFS)*, 11(10):2268–2283, 2016. 1, 2

[49] Jason Phang, Thibault Févry, and Samuel R. Bowman. Sentence encoders on stilts: Supplementary training on intermediate labeled-data tasks. *arXiv preprint arXiv:1811.01088*, 2018. 16

[50] Yunxiao Qin, Chenxu Zhao, Xiangyu Zhu, Zezheng Wang, Zitong Yu, Tianyu Fu, Feng Zhou, Jingping Shi, and Zhen Lei. Learning meta model for zero-and few-shot face antispoofing. In *Association for the Advancement of Artificial Intelligence (AAAI)*, 2020. 3, 15

[51] Sachin Ravi and Hugo Larochelle. Optimization as a model for few-shot learning. In *International Conference on Learning Representations (ICLR)*, 2017. 3

[52] Suman Saha, Wenhao Xu, Menelaos Kanakis, Stamatios Georgoulis, Yuhua Chen, Danda Pani Paudel, and Luc Van Gool. Domain agnostic feature learning for image and video based face anti-spoofing. In *IEEE Conference on Computer Vision and Pattern Recognition Workshops (CVPRW)*, 2020. 3, 15

[53] Rui Shao, Xiangyuan Lan, Jiawei Li, and Pong C. Yuen. Multi-adversarial discriminative deep domain generalization for face presentation attack detection. In *IEEE Conference on Computer Vision and Pattern Recognition (CVPR)*, 2019. 2, 3, 15

[54] Rui Shao, Xiangyuan Lan, and Pong C. Yuen. Regularized fine-grained meta face anti-spoofing. In *Association for the Advancement of Artificial Intelligence (AAAI)*, 2020. 3, 15

[55] Jake Snell, Kevin Swersky, and Richard Zemel. Prototypical networks for few-shot learning. In *Neural Information Processing Systems (NeurIPS)*, 2017. 3

[56] Flood Sung, Yongxin Yang, Li Zhang, Tao Xiang, Philip HS Torr, and Timothy M Hospedales. Learning to compare: Relation network for few-shot learning. In *IEEE Conference on Computer Vision and Pattern Recognition (CVPR)*, 2018. 3

[57] Takeshi Teshima, Issei Sato, and Masashi Sugiyama. Few-shot domain adaptation by causal mechanism transfer. In *International Conference on Machine Learning (ICML)*, 2020. 3

[58] Hung-Yu Tseng, Hsin-Ying Lee, Jia-Bin Huang, and Ming-Hsuan Yang. Cross-domain few-shot classification via learned feature-wise transformation. In *International Conference on Learning Representations (ICLR)*, 2020. 3, 5

[59] Laurens van der Maaten and Geoffrey Hinton. Viualizing data using t-sne. *Journal of Machine Learning Research (JMLR)*, 9:2579–2605, 2008. 9, 23

[60] Oriol Vinyals, Charles Blundell, Timothy Lillicrap, koray kavukcuoglu, and Daan Wierstra. Matching networks for one shot learning. In *Neural Information Processing Systems (NeurIPS)*, 2016. 3

[61] Guoqing Wang, Hu Han, Shiguang Shan, and Xilin Chen. Cross-domain face presentation attack detection via multi-domain disentangled representation learning. In *IEEE Conference on Computer Vision and Pattern Recognition (CVPR)*, 2020. 3, 15

[62] Jingjing Wang, Jingyi Zhang, Ying Bian, Youyi Cai, Chunmao Wang, and Shiliang Pu. Self-domain adaptation for face anti-spoofing. In *Association for the Advancement of Artificial Intelligence (AAAI)*, 2021. 3, 7, 15

[63] Yu-Xiong Wang, Ross Girshick, Martial Hebert, and Bharath Hariharan. Low-shot learning from imaginary data. In *IEEE Conference on Computer Vision and Pattern Recognition (CVPR)*, 2018. 3

[64] Di Wen, Hu Han, and Anil K Jain. Face spoof detection with image distortion analysis. *Transactions on Information Forensics and Security (TIFS)*, 10(4):746–761, 2015. 2, 6

[65] Xiang Xu, Xiong Zhou, Ragav Venkatesan, Gurumurthy Swaminathan, and Orchid Majumder. d-sne: Domain adaptation using stochastic neighborhood embedding. In *IEEE Conference on Computer Vision and Pattern Recognition (CVPR)*, 2019. 3

[66] Bowen Yang, Jing Zhang, Zhenfei Yin, and Jing Shao. Few-shot domain expansion for face anti-spoofing. *arXiv preprint arXiv:2106.14162*, 2021. 3

[67] Jianwei Yang, Zhen Lei, and Stan Z Li. Learn convolutional neural network for face anti-spoofing. *arXiv preprint arXiv:1408.5601*, 2014. 2

[68] Jianwei Yang, Zhen Lei, Shengcai Liao, and Stan Z Li. Face liveness detection with component dependent descriptor. In *International Confernece on Biometrics (ICB)*, 2013. 2

[69] Xiao Yang, Wenhan Luo, Linchao Bao, Yuan Gao, Dihong Gong, Shibao Zheng, Zhifeng Li, and Wei Liu. Face anti-spoofing: Model matters, so does data. In *IEEE Conference on Computer Vision and Pattern Recognition (CVPR)*, 2019. 4

[70] Zitong Yu, Xiaobai Li, Xuesong Niu, Jingang Shi, and Guoying Zhao. Face anti-spoofing with human material perception. In *European Conference on Computer Vision (ECCV)*, 2020. 2

[71] Zitong Yu, Yunxiao Qin, Xiaqing Xu, Chenxu Zhao, Zezheng Wang, Zhen Lei, and Guoying Zhao. Auto-fas: Searching lightweight networks for face anti-spoofing. In *IEEE International Conference on Acoustics, Speech and SP (ICASSP)*, 2020. 2

[72] Zitong Yu, Yunxiao Qin, Hengshuang Zhao, Xiaobai Li, and Guoying Zhao. Dual-cross central difference network for face anti-spoofing. In *International Joint Conference on Artificial Intelligence (IJCAI)*, 2021. 18

[73] Zitong Yu, Jun Wan, Yunxiao Qin, Xiaobai Li, S. Li, and Guoying Zhao. Nas-fas: Static-dynamic central difference network search for face anti-spoofing. *IEEE Transactions on Pattern Recognition and Machine Intelligence (PAMI)*, 43:3005–3023, 2021. 2, 7, 15

[74] Zitong Yu, Chenxu Zhao, Zezheng Wang, Yunxiao Qin, Zhuo Su, Xiaobai Li, Feng Zhou, and Guoying Zhao. Searching central difference convolutional networks for face anti-spoofing. In *IEEE Conference on Computer Vision and Pattern Recognition (CVPR)*, 2020. 18

[75] Ke-Yue Zhang, Taiping Yao, Jian Zhang, Ying Tai, Shouhong Ding, Jilin Li, Feiyue Huang, Haichuan Song, and Lizhuang Ma. Face anti-spoofing via disentangled representation learning. In *European Conference on Computer Vision (ECCV)*, 2020. 2

[76] Shifeng Zhang, Ajian Liu, Jun Wan, Yanyan Liang, Guodong Guo, Sergio Escalera, Hugo Jair Escalante, and Stan Z. Li. Casia-surf: A large-scale multi-modal benchmark for face anti-spoofing. *IEEE Transactions on Biometrics, Behavior, and Identity Science (T-BIOM)*, 2020. 6

[77] Shifeng Zhang, Xiaobo Wang, Ajian Liu, Chenxu Zhao, Jun Wan, Sergio Escalera, Hailin Shi, Zezheng Wang, and Stan Z. Li. A dataset and benchmark for large-scale multi-modal face anti-spoofing. In *IEEE Conference on Computer Vision and Pattern Recognition (CVPR)*, 2019. 6

[78] Xueting Zhang, Debin Meng, Henry Gouk, and Timothy M. Hospedales. Shallow bayesian meta learning for real-world few-shot recognition. In *IEEE International Conference on Computer Vision (ICCV)*, 2021. 3

[79] Yuanhan Zhang, Zhenfei Yin, Yidong Li, Guojun Yin, Junjie Yan, Jing Shao, and Ziwei Liu. Celeba-spoof: Large-scale face anti-spoofing dataset with rich annotations. In *European Conference on Computer Vision (ECCV)*, 2020. 6, 19

[80] Zhiwei Zhang, Junjie Yan, Sifei Liu, Zhen Lei, Dong Yi, and Stan Z Li. A face antispoofing database with diverse attacks. In *International Confernece on Biometrics (ICB)*, 2012. 2, 6

[81] Kaiyang Zhou, Yongxin Yang, Yu Qiao, and Tao Xiang. Domain generalization with mixstyle. In *International Conference on Learning Representations (ICLR)*, 2021. 17

Appendix

In this appendix, we first discuss implementation and experiment details. Next, we present more ablation studies of our approach. Third, we provide additional visualization to validate the proposed design. Finally, we include additional discussions.

A Implementation Details

Frame sampling strategy for Protocol 1. Following SSDG [22], we train the model using only one frame selected in each video, and evaluate the model using two frames in each video. Both the training and test set videos in the original dataset are considered as data in one domain, and there are no training and test splits for cross-domain evaluation. We hold out ten frames in each domain as the few-shot samples. We calculate the average probability for each video and the HTER, AUC and TPR@FPR=1% scores are obtained based on videos instead of frames. We use TPR@FPR=1% as the metric instead of TPR@FPR=0.1% since the test sets contain only hundreds of images.

Frame sampling strategy for Protocol 2. We train the model using ten frames equidistantly sampled from each video, and evaluate the model using ten frames in each video for WMCA and CeFA. We use all frames from the SURF dataset. We split the data into training and test sets for this protocol. As there are multiple spoof types in WMCA dataset, we use all videos for training, and use only print attacks, replay attacks and live videos for test. For CeFA and SURF datasets, we use all data as training set, and use the original validation set for test. We hold out ten frames in each domain as the few-shot samples. As SURF does not contain videos, we calculate the HTER, AUC and TPR@FPR=1% scores based on the probabilities of frames instead of videos. Based on the sampling strategy, the numbers of frames used in training/test are 16K/9K (WMCA), 60K/12K (CeFA) and 96K/9K (SURF).

Explanation about the benchmark. We follow the typical cross-domain evaluation setting that is widely used in face anti-spoofing literature [53, 22, 52, 24, 54, 7, 62, 61, 38, 73, 37, 35]. We note that the zero-shot benchmark proposed in [40] has been previously retrieved and is no longer available. The benchmark proposed in [50] is less used in the FAS literature. The authors study a different topic of detecting novel live/spoof sub-categories, and their zero/few-shot settings use ten live and spoof samples from two different sub-categories for adaptation. The problem setup is different from our supervised few-shot domain adaptation task.

We report the comparison to [50] in Table 3 following their training/test protocols. Instead of using their meta-learning approach, we simply train the model with binary classification loss using the training set. At test time, we follow their zero/few-shot evaluation settings and use a balanced data batch formed by the few-shot samples and the samples from the training set to adapt the model. All models are initialized from the ImageNet-pretrained ViT and fine-tuned following the data splits in their benchmark. Our model performs favorably against [50], especially for the few-shot settings.

Table 3: **ACER** (%) **Comparison to [50]**. We report the results on the benchmarks proposed in [50]. Our model performs favorably against prior work, especially for the few-shot settings.

Benchmark	Method	0-shot	1-shot	5-shot
OULU-ZF	[50]	4.97±1.29	4.00±1.31	2.44±0.71
	Ours	**4.96±1.18**	**3.66±1.16**	**1.60±0.53**
SURF-ZF	[50]	30.97 ±1.28	28.75 ±1.49	27.27±1.25
	Ours	**28.53±2.48**	**22.50±2.33**	**21.60 ±2.95**

B More Ablation Studies

B.1 Analysis of the Adaptive Module

As discussed in the paper, fine-tuning large models such as ViT with few samples usually causes instability. The proposed adaptive transformer model allows the transformer to operate on fewer

parameters with a skip-connection to reduce optimization difficulty, thus achieving stability for mitigating domain gap in face anti-spoofing. Here we provide more analysis to justify the effectiveness of the proposed adaptive transformer model.

First, we plot the loss landscapes [31] of the naive ViT and our adaptive transformer in Fig. 8(a). The loss landscape by ViTAF* is wide and flat compared to the naive ViT, which indicates better generalization. Second, as discussed in Section 4.3 and Fig. 3 of the paper, the fine-tuning test performance of ViT model may fluctuate among different checkpoints even when the training loss converges. In Fig. 8(b), we show the learning curve of the ViT method and the proposed ViTAF* method. Although the best performance of ViT is already comparable to state-of-the-art, the performance fluctuates among different checkpoints and saturates since early iterations. In contrast, the test performance by the ViTAF* model gradually increases when it is trained for longer iterations, and there is no large fluctuation among the checkpoints. The learning curve validates the robust performance achieved by the ensemble adapters. Third, the skip-connection in the adapter module makes the output embedding mimic the input embedding, which yields representations with less deviation from the pre-trained ones and alleviates the instability caused by the catastrophic forgetting problem [49, 12, 29]. In Fig. 8(c), we plot the representational similarity [28] between the ImageNet-pretrained ViT and the fine-tuned ViT (blue line) versus the similarity between the ImageNet-pretrained ViT and the fine-tuned ViTAF* (orange line). The results show that the proposed model has higher feature similarity, thus indicating that ViTAF* better alleviates the catastrophic forgetting problem to achieve training stability.

(a) Loss landscapes

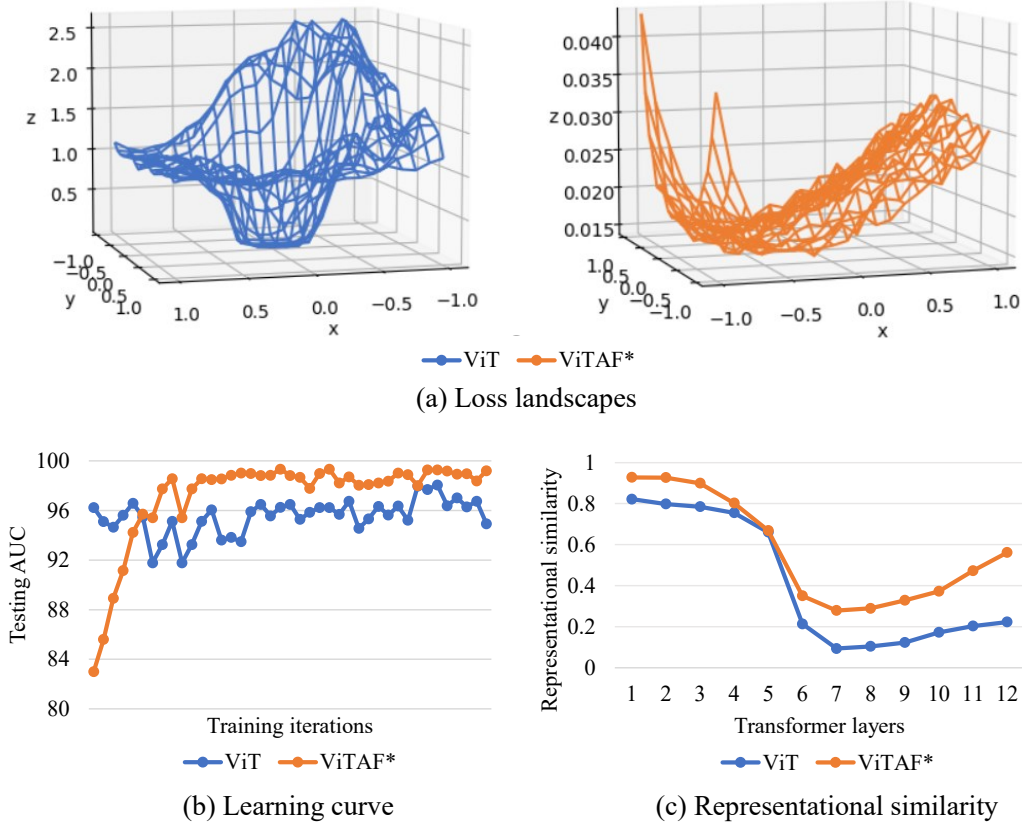(b) Learning curve

(c) Representational similarity

Figure 8: **Analysis of the adaptive module.** (a) The loss landscape of ViTAF* is wide and flat compared to naive ViT. (b) The test AUC of ViTAF* stably increases during the training process. (c) The representational similarity of ViTAF* is higher, indicating ViTAF* better alleviates the catastrophic forgetting problem.

B.2 Ablation Study of Number of Ensemble Adapters

In the experiments presented in the manuscript, we set the number of adapters in the ensemble adapter module as $K = 2$. In Table 4, we present the results of using different numbers of adapters in the ensemble module. While the ensemble module can be extended to include more than two adapters, we do not observe consistent improvements when increasing the number of adapters to $K = 3$ and $K = 4$. Thus, we keep $K = 2$ in the paper.

In addition, we include the results of ablating the cosine similarity loss L_{cos} in our framework. We observe that no matter how many adapters are used in the ensemble modules, the performance drop when we remove L_{cos}, which suggests that L_{cos} is essential for the multiple adapters to learn diverse feature and improve the accuracy.

Table 4: **Ablation study of number of ensemble adapters.** Increasing the number of adapters to $K = 3$ or $K = 4$ does not bring consistent improvements to the model. Removing the L_{cos} causes the AUC drop for all cases.

	OCI → M			OMI → C			OCM → I			ICM → O		
	HTER	AUC	TPR@ FPR=1%	HTER	AUC	TPR@ FPR=1%	HTER	AUC	TPR@ FPR=1%	HTER	AUC	TPR@ FPR=1%
K=1	3.42	99.30	88.33	1.40	99.85	95.71	3.74	99.34	85.38	7.17	98.26	71.97
K=2 (Ours)	2.92	**99.62**	**91.66**	1.40	**99.92**	**98.57**	1.64	99.64	91.53	5.39	98.67	76.05
K=3	2.92	99.80	93.33	2.91	99.64	92.14	**1.35**	**99.88**	**98.46**	6.04	98.78	**83.38**
K=4	**1.58**	99.51	91.66	2.09	99.81	95.00	1.42	99.88	96.15	**5.36**	**98.87**	78.87
K=2 $w/o\ L_{cos}$	5.00	98.58	88.33	3.02	99.45	87.86	3.81	99.20	86.15	7.04	98.02	71.27
K=3 $w/o\ L_{cos}$	5.00	98.80	83.33	2.90	99.55	86.42	2.29	99.44	84.61	5.56	98.55	69.43
K=4 $w/o\ L_{cos}$	3.42	98.89	86.67	1.51	99.73	92.14	2.09	99.64	90.00	6.93	98.38	78.59

B.3 Comparison to Feature-level Augmentation Methods

In our adaptive transformer model, we utilize the feature-wise transformation layer as we find its usefulness for cross-domain anti-spoofing task. We do not claim that we proposed the most effective augmentation approach. In Table 5, we compare our methods to two representative feature-level augmentation methods for domain generalization, DropBlock [18] and MixStyle [81]. The two methods are not directly applicable to ViT and we add these approaches to our baseline SSDG for comparison. Although these feature augmentation methods [18, 81] achieve good performance on standard cross-domain object classification benchmark [30], the results show that our model is more effective for the face anti-spoofing domain.

Table 5: **Comparison to feature-level augmentation methods.** We compare our model to representative feature-level augmentation approaches [18, 81]. The results show that our model is more effective for few-shot cross-domain anti-spoofing.

Method	OCI → M		OMI → C		OCM → I		ICM → O	
	HTER	AUC	HTER	AUC	HTER	AUC	HTER	AUC
SSDG	8.42	97.39	12.91	93.59	4.48	99.14	7.81	97.46
SSDG+DropBlock	3.41	99.13	14.30	93.79	6.12	98.75	9.56	97.05
SSDG+MixStyle	5.00	97.63	6.51	97.35	3.06	99.54	10.26	96.23
ViTAF*	**2.92**	**99.62**	**1.40**	**99.92**	**1.64**	**99.64**	**5.39**	**98.67**

B.4 Ablation Study of Increasing Few-shot Samples

In Fig. 9, we conduct an ablation study of increasing the number of few-shot target domain samples provided at training time. The x-axis shows the number of few-shot samples including 5-shot, 10-shot, 20-shot, 50-shot, 100-shot and all-shot. The y-axis shows the TPR@FPR=1% metric. Note that to conduct this experiment, we split the datasets into training and test sets, and thus the result is not directly comparable to the results in the main paper. We observe that the TPR@FPR=1% scores increase when more few-shot samples are included in training for all datasets. In addition, the TPR@FPR=1% score achieves 90% (which is almost saturated) when there are 5 shots (OCI → M), 10 shots (OMI → C), 20 shots (OCM → I), 100 shots (ICM → O), 50 shots (CS → W), 50 shots (SW → C) and 20 shots (CW → S). The results suggest that including less than 5% samples in the target domain at training time can achieve good performance.
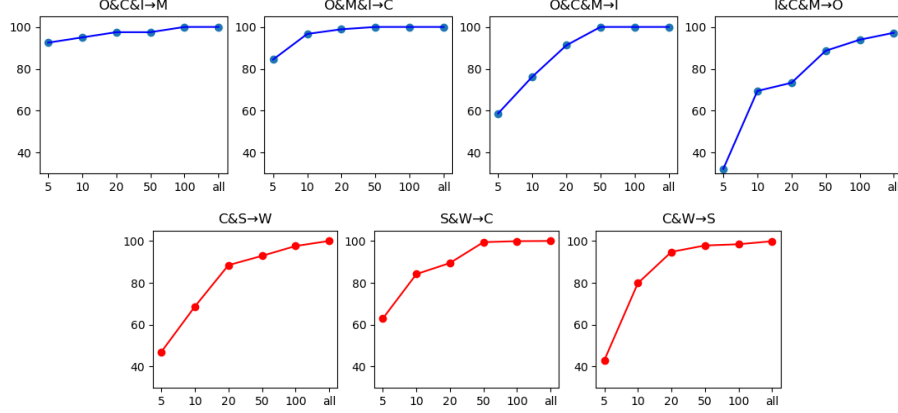
Figure 9: **Ablation study of increasing few-shot samples.** We conduct ablation study of increasing the number of few-shot target domain samples provided at training time. The x-axis shows the number of few-shot samples from 5-shot to 100-shot and all-shot in log scale. The y-axis shows the TPR@FPR=1% metric.

B.5 Intra-database Evaluation

To continue the discussion in the previous section, we provide the intra-database results on four protocols of the Oulu-NPU dataset in Table 6. Although our approach does not aim at intra-database evaluation where the training/test sets are from the same domain, our method achieves performance comparable to the state-of-the-art method DC-CDN [72] for protocol 2 and 3, and it obtains favorable results for protocol 1 and 4.

Table 6: **Intra-database evaluation on Oulu-NPU dataset.** Our method is comparable to the state-of-the-art method for protocol 2 and 3, and it achieves favorable results for protocol 1 and 4.

Prot.	Method	APCER(%)↓	BPCER(%)↓	ACER(%)↓
1	CDCN [74]	0.4	1.7	1.0
	DC-CDN [72]	0.5	0.3	**0.4**
	Ours	0.4	1.8	1.1
2	CDCN [74]	1.5	1.4	1.5
	DC-CDN [72]	0.7	1.9	1.3
	Ours	1.1	1.1	**1.1**
3	CDCN [74]	2.4	2.2	2.3
	DC-CDN [72]	2.2	1.6	**1.9**
	Ours	0.4	3.3	**1.9**
4	CDCN [74]	4.6	9.2	6.9
	DC-CDN [72]	5.4	2.5	**4.0**
	Ours	0.0	15.0	7.5

B.6 Ablation Study of Using Different 5-shot Samples

In our experiments in the paper, the 5-shot samples of the target domains are selected randomly and fixed for all the experiments. In Table 7, we provide an ablation study of using different sets of 5-shot samples randomly selected from the target domain. We conduct the experiments for five runs and report the average performance and standard deviation.

The standard deviation of AUC score in five runs are: 0.27 (OCI $\rightarrow$ M), 0.50 (OMI $\rightarrow$ C), 0.98 (OCM $\rightarrow$ I), 0.36 (ICM $\rightarrow$ O), 0.33 (CS $\rightarrow$ W), 0.64 (SW $\rightarrow$ C), 1.87 (CW $\rightarrow$ S). Although the performance varies due to the selection of 5-shot samples, the variation is not large for most datasets. There are higher variations for Idiap (I), CeFA (C) and SURF (S). The datasets CeFA (C) and SURF (S) have 10$\times$ more examples than other datasets and the 5-shot samples cover only 0.1% of the data. Therefore, using different sets of 5-shot samples leads to a larger performance variation for SW $\rightarrow$ C and CW $\rightarrow$ S. On the other hand, OCM $\rightarrow$ I also has a larger performance variation caused by the selection of 5-shot samples. This might be due to the low resolution (480P) of the Idiap (I)

dataset which causes some live videos to have even worse visual quality than spoof videos, and the recording environments are less diverse than other datasets. Therefore, if the selected 5-shot samples are outliers that do not cover the common live/spoof types, the model will be biased and the performance degrades. We note that although in Protocol 2 there are seven kinds of spoof attacks in the WMCA (W) dataset, we have only used replay and print attacks for testing. Thus, the 5-shot selection strategy is not an issue for CS → W as shown in Table 7. More details about the frame sampling strategy are in Section A. It is interesting to study which samples obtained from the new domain are most beneficial for the few-shot adaptation, which we leave as future work.

Table 7: **Ablation study of using different 5-shot samples.** In our experiments in the paper, the 5-shot samples of each dataset are selected randomly and fixed for all the experiments. Here we provide an ablation study of using different sets of 5-shot samples randomly selected in the target domain. We conduct the experiments for five runs and report the average results and standard deviation.

	OCI → M			OMI → C			OCM → I			ICM → O		
	HTER	AUC	TPR@FPR=1%	HTER	AUC	TPR@FPR=1%	HTER	AUC	TPR@FPR=1%	HTER	AUC	TPR@FPR=1%
Mean	2.37	99.55	91.53	3.14	99.34	86.64	5.60	98.68	72.77	8.33	97.68	64.79
Std	1.26	0.27	3.69	1.47	0.50	9.00	3.15	0.98	17.08	0.74	0.36	5.42

		CS → W			SW → C			CW → S		
		HTER	AUC	TPR@FPR=1%	HTER	AUC	TPR@FPR=1%	HTER	AUC	TPR@FPR=1%
	Mean	4.31	99.32	86.51	6.51	98.20	68.76	9.31	96.15	66.76
	Std	1.19	0.33	6.58	1.50	0.64	10.38	2.65	1.87	12.84

B.7 Ablation Study of Excluding CelebA-Spoof

Table 8 shows the ablation study of excluding CelebA-Spoof [79] from the source datasets. We present the results of our 0-shot ViT and 5-shot ViTAF model. ViT[†] and ViTAF[†] denote the model trained without using CelebA-Spoof in the source datasets. Excluding CelebA-Spoof causes the performance drop in all target datasets for the 0-shot ViT model, and six out of seven target datasets for the 5-shot ViTAF model. These results show that including CelebA-Spoof in the source datasets increases the diversity of training data and helps learn a better representation.

The 0-shot ViT[†] has an average 6.38 AUC performance drop compared to 0-shot ViT, while 5-shot ViTAF[†] has a 1.31 AUC drop compared to 5-shot ViTAF. The results suggest that when there are no target domain samples provided at training time, the diversity of source datasets highly affects the results. On the other hand, when there are few-shot samples, excluding CelebA-Spoof does not cause a drastic performance drop, though still a moderate difference, which shows the effectiveness of CelebA-Spoof dataset on improving the generalizability of the model.

Table 8: **Ablation study of excluding CelebA-Spoof.** We present the ablation study of excluding CelebA-Spoof [79] from the source datasets. We present the results of our 0-shot ViT and 5-shot ViTAF model. ViT[†] and ViTAF[†] denote the model trained without using CelebA-Spoof as the supplementary source dataset.

	Method	OCI→M			OMI→C			OCM→I			ICM→O		
		HTER	AUC	TPR@FPR=1%	HTER	AUC	TPR@FPR=1%	HTER	AUC	TPR@FPR=1%	HTER	AUC	TPR@FPR=1%
0-shot	ViT	1.58	99.68	96.67	5.70	98.91	88.57	9.25	97.15	51.54	7.47	98.42	69.30
	ViT[†]	4.75	98.79	68.33	15.70	92.76	36.43	17.68	86.66	50.77	16.46	90.37	24.23
5-shot	ViTAF	3.42	99.30	88.33	1.40	99.85	95.71	3.74	99.34	85.38	7.17	98.26	71.97
	ViTAF[†]	4.75	98.59	80.00	4.19	98.59	57.86	3.28	99.27	76.92	10.74	95.70	51.13

	Method	CS→W			SW→C			CW→S		
		HTER	AUC	TPR@FPR=1%	HTER	AUC	TPR@FPR=1%	HTER	AUC	TPR@FPR=1%
0-shot	ViT	7.98	97.97	73.61	11.13	95.46	47.59	13.35	94.13	49.97
	ViT[†]	21.04	89.12	30.09	17.12	89.05	22.71	17.16	90.25	30.23
5-shot	ViTAF	4.51	99.44	88.23	7.21	97.69	70.87	11.74	94.13	50.87
	ViTAF[†]	4.91	98.78	75.95	13.56	93.68	30.90	12.63	94.21	55.03

B.8 Ablation Study of Alternative Transfer Learning Strategies

As discussed in Section 3.2 in the paper, one straightforward transfer learning strategy is to train a classifier on top of features extracted by the ViT backbone pre-trained on ImageNet [11] using anti-spoofing data. Another common strategy is to freeze a majority of the backbone and partially fine-tune the network. In Table 9, we investigate the transfer learning strategies on ViT models by comparing several alternatives: (1) ViT (fixed): fixing the ViT backbone and fine-tuning only the MLP head; (2) ViT (fine-tune last four): fine-tuning the last four layers along with the MLP head; (3) ViT (fine-tune last eight): fine-tuning the last eight layers.

The result shows that our transfer learning strategy outperforms the other alternatives where only parts of the network are fine-tuned. It also validates that fine-tuning the introduced ensemble adapters and feature-wise transformation layers effectively adapts the features of ViT to the anti-spoofing tasks. In addition, only fine-tuning the MLP head on top of a fixed ViT backbone leads to degraded performance, suggesting that ImageNet-pretrained ViT features are high-level thus cannot be directly used for anti-spoofing tasks where the subtle low-level information is crucial.

Table 9: **Ablation study of alternative transfer learning strategies.** The alternative strategies include: (1) ViT (fixed): fixing the ViT backbone and fine-tuning only the MLP head; (2) ViT (fine-tune last four): fine-tuning the last four layers along with the MLP head; (3) ViT (fine-tune last eight): fine-tuning the last eight layers.

	OCI → M			OMI → C			OCM → I			ICM → O		
	HTER	AUC	TPR@ FPR=1%	HTER	AUC	TPR@ FPR=1%	HTER	AUC	TPR@ FPR=1%	HTER	AUC	TPR@ FPR=1%
ViT (fixed)	13.66	93.55	45.00	21.39	87.23	38.57	20.81	86.89	30.77	19.44	88.61	26.06
ViT (fine-tune last four)	6.83	98.00	68.33	10.69	95.52	49.29	9.32	95.99	52.31	11.69	94.86	50.99
ViT (fine-tune last eight)	3.41	98.63	80.00	5.69	98.33	70.71	6.12	98.31	66.15	12.03	95.50	40.56
ViTAF*	**2.92**	**99.62**	**91.66**	**1.40**	**99.92**	**98.57**	**1.64**	**99.64**	**91.53**	**5.39**	**98.67**	**76.05**

B.9 ViTF in 0-shot Setting

In the proposed framework, both the ensemble adaptor modules and the FWT layers are specifically designed and suitable for the few-shot domain adaptation problem. On the other hand, the ViTF model with FWT layers can be served as a general feature-wise augmentation method and applied to the 0-shot setting when there are no target domain samples available. We include the results of ViTF model in 0-shot setting in Table 10. We observe that the ViTF model does not have improvements compared to ViT for the setting **ICM→O**. A possible reason is **O** has a more diverse distribution than other datasets in protocol 1. Thus, the data augmentation on the source datasets **ICM** does not bring improvement to the target **O**.

Table 10: **ViTF in 0-shot setting.** Including the FWT layer does not bring improvement to ICM→O in 0-shot setting.

Method	OCI → M		OMI → C		OCM → I		ICM → O	
	HTER	AUC	HTER	AUC	HTER	AUC	HTER	AUC
SSDG	6.58	97.21	12.91	93.92	7.01	98.28	12.47	94.87
ViT	**1.58**	99.68	5.70	98.91	9.25	97.15	**7.47**	**98.42**
ViTF	2.20	**99.74**	**4.89**	**99.21**	**6.12**	**98.55**	7.89	97.58

B.10 Runtime Analysis and Network Comparison

In Table 11, we show the training and inference time of the proposed method, the details of network sizes and the computational complexity. The analysis is conducted on a desktop machine equipped with an Nvidia 2080Ti GPU. We show that the network parameters and the computational complexity of the ViTAF* model increase only ≈ 5.5% compared to the naive ViT model. The analysis shows that the proposed ensemble adapter modules and the feature-wise transformation layers are lightweight. In practice, the training time and inference time of ViTAF* increase only 15% compared to the ViT model. Overall, it takes three hours to finish the training/evaluation for protocol 1, and six hours for protocol 2.

Table 11: **Run-time analysis.** We present the training, inference time, network sizes and computational complexity of the proposed method.

Pre-training time (seconds / per iteration)	ViT/ViTAF*	0.17
Fine-tuning time (seconds / per iteration)	ViT ViTAF*	0.18 0.21 (+15%)
Inference time (seconds / per input frame)	ViT ViTAF*	0.013 0.015 (+15%)
Number of parameters	ViT ViTAF*	86.39M 91.15M (+5.5%)
FLOPs	ViT ViTAF*	33.69G 35.56G (+5.5%)

C Visualization

ROC curves. The ROC curves represent equivalent information as the AUC scores provided in the paper. In Fig. 10 we plot the ROC curves of our method and the baseline model SSDG for reference.
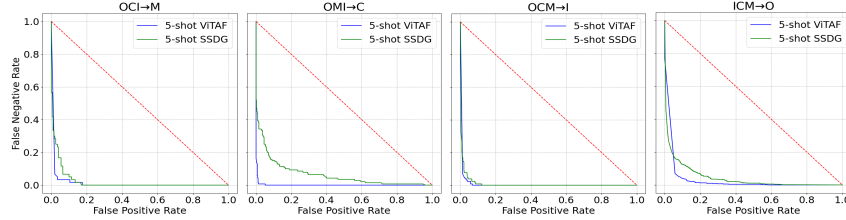
Figure 10: **ROC curves.** We compare the ROC curves of our method and the SSDG baseline for protocol 1.

Failure cases. In Fig. 11, we provide additional failure case analysis for Protocol 2. The live faces misclassified as spoof faces are shown in blue boxes and the spoof faces misclassified as live faces are shown in red boxes. The live faces misclassified as spoof faces (blue) are in dark light conditions (top left), or have bad visual quality and larger pose changes (top right). In addition, the live faces with darker skin are more challenging (example shown in the top middle). The spoof faces misclassified as live faces (red) are mostly replay attacks without obvious spoof cues for $\mathbf{CS} \to \mathbf{W}$. As for $\mathbf{SW} \to \mathbf{C}$, faces printed on clothes in either indoor or outdoor light conditions are the most challenging spoof types as there are no obvious spoof cues. The most challenging spoof type for $\mathbf{CW} \to \mathbf{S}$ is the person holding curved photos with good visual quality. Since images in the SURF dataset generally have low resolution and bad visual quality, the spoof faces with better quality are easily misclassified as live.
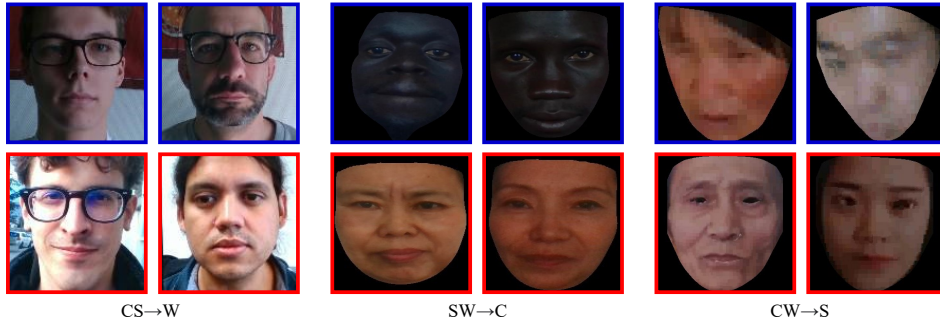

Figure 11: **Failure case analysis for Protocol 2.** We provide additional failure case analysis. The live faces misclassified as spoof faces are shown in blue boxes and the spoof faces misclassified as live faces are shown in red boxes.

Attention maps. As shown in Fig. 12, we visualize the attention maps of different transformer models on spoof images using Transformer Explainability [6]. We observe that different regions are highlighted by transformers to make predictions for different spoof face domains. For example, transformers make predictions mainly based on the paper boundaries or reflection on screens for paper and replay attack in $\mathbf{CS} \rightarrow \mathbf{W}$. For attacks printed on clothes, transformers focus on the wrinkles in $\mathbf{SW} \rightarrow \mathbf{C}$. As for the paper attacks where eye or nose regions are cut out in $\mathbf{CW} \rightarrow \mathbf{S}$, transformers pay more attention to the cut regions (holes) on the spoof medium. Moreover, our methods can better capture the spoof cues compared to the naive ViTs, as the attention region given by our models is more conspicuous.
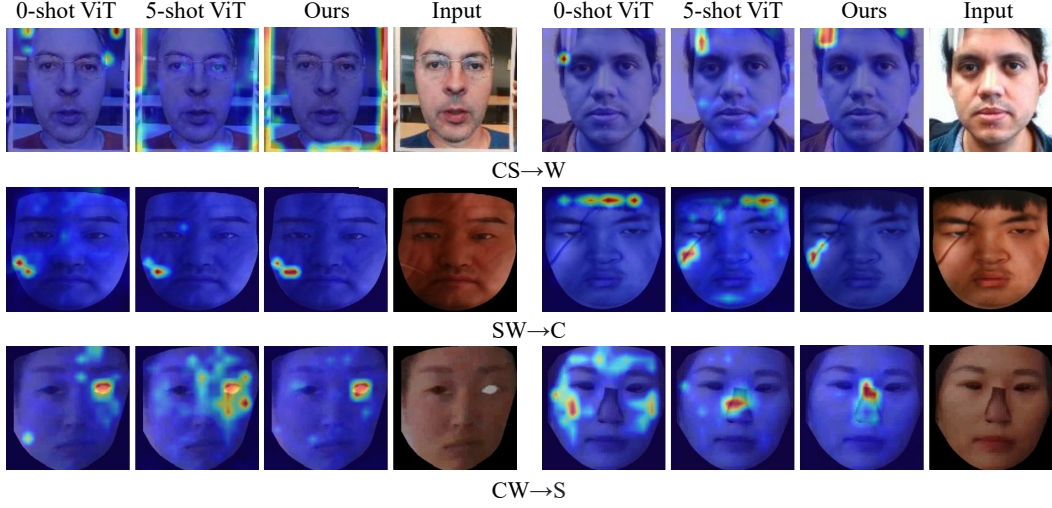

Figure 12: **Transformer attention on spoof images for Protocol 2.** We visualize the attention maps of transformers using Transformer Explainability [6] and make a comparison of naive ViT and our models. Transformers focus on paper boundaries or reflection on screens ($\mathbf{CS} \rightarrow \mathbf{W}$), clothes wrinkles ($\mathbf{SW} \rightarrow \mathbf{C}$), holes at eye or nose regions ($\mathbf{CW} \rightarrow \mathbf{S}$). Our models generate more accurate and conspicuous attention maps to capture spoof cues compared with others.
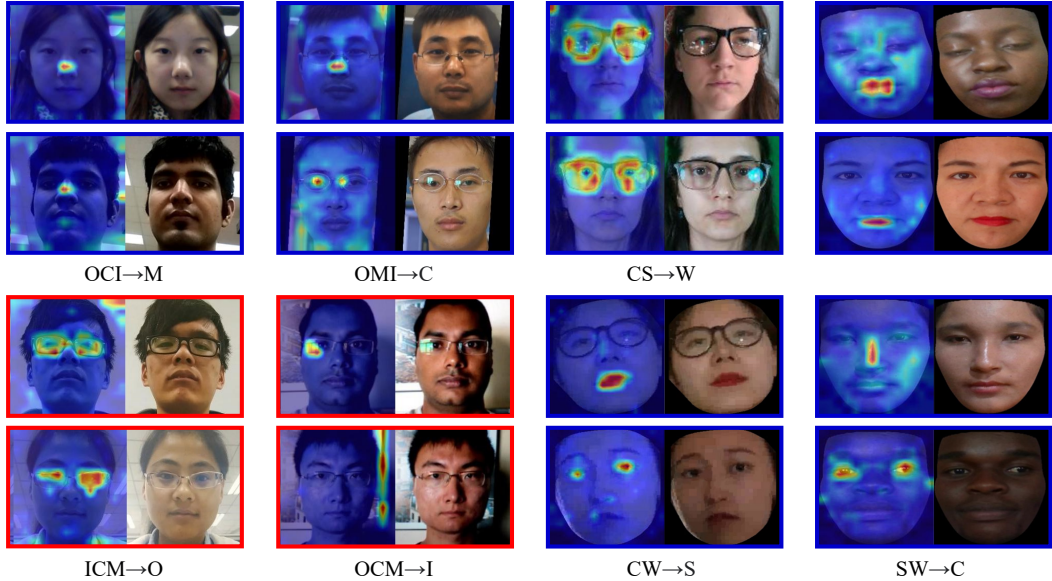

Figure 13: **Additional results.** We provide additional visualization of the attention maps. Live or spoof faces are shown in blue or red boxes.

In Fig. 13, we provide additional visualization of attention. Live or spoof faces are shown in blue or red boxes. Transformer focuses on reflection light on noses for live faces in **OCI → M** and **OMI → C**. The reflection light on noses is usually a cue of live faces. In addition, transformer focuses on reflections on glasses and boundaries of the painting on the background for **OCM → I**. Though glasses or painting on the background are not spoof cues, the reflection on glasses is similar to the reflections caused by replay attacks, and the painting boundaries look similar to the boundaries of spoof mediums. Our model focuses on glasses region for **OMI → C**, **ICM → O** and **CS → W** as well. As for the live faces in **CW → S** and **SW → C**, transformer model mainly focuses on eyes, nose, and mouth region which usually show cues for live faces.

Feature visualization of Protocol 2. We present the t-SNE plot [59] of Protocol 2 in Fig. 14. Each plot indicates the features extracted from the model of each setting shown on the top. Each color in the plot shows the live/spoof samples in each dataset. We observe that features of WMCA (purple, brown) extracted from model **CS → W** (left) are well-separated, demonstrating that the model generalizes well to the target domain. In addition, features of CeFA (blue, orange) extracted from model **SW → C** (middle) are almost but not entirely separated, indicating there is still room of improvement for this model. On the other hand, features of SURF (green, red) extracted from model **CW → S** (right) are mixed. Since images in SURF have very low visual quality, the model trained on CW does not generalize well to S.
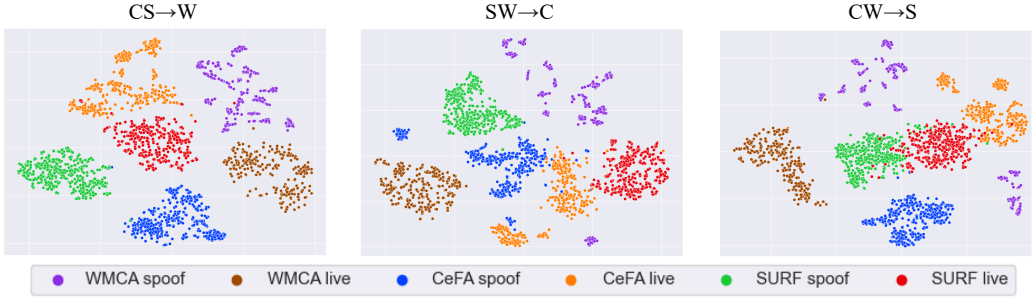

Figure 14: **Feature visualization of Protocol 2.** We present the t-SNE plot of Protocol 2. Each plot indicates the features extracted from the model of each setting shown on the top. Each color in the plot shows the live/spoof samples in each dataset.

D   Discussions

Although adapter methods are recently developed in natural language processing (NLP), our paper aims at the face anti-spoofing problem in computer vision, which is significantly different from NLP. We develop the first method to successfully apply the adaptive module to vision transformers for face anti-spoofing domain, especially for the cross-domain FAS task. Our adaptive transformer model effectively adapts the pre-trained model to novel domains with only a few samples available. Therefore, it is a promising direction for face anti-spoofing domain where the data is usually hard to obtain.

It is challenging to apply the adaptive module to cross-domain face anti-spoofing task. We introduce the ensemble adaptive module with the cosine loss which is essential to achieve the stable and good performance. We believe that our findings are worth sharing with the face anti-spoofing community.